Article

Reduced Graphene Oxide/Ruthenium Oxide Hexacyanoferrate Nanocomposite for Electrochemical Determination of Ethanol in Commercial Samples

Pedro H. S. Borges[a] and Edson Nossol [iD] *,[a]

[a]*Instituto de Química, Universidade Federal de Uberlândia, 38400-902 Uberlândia-MG, Brazil*

Reduced graphene oxide/ruthenium oxide hexacyanoferrate (rGO/RuOHCF) modified electrode showed synergic activity between the materials attested by the increase of electrochemical current and stability. The preparation of the nanocomposite was made by a simple two-step electrochemical approach. The material structure was characterized by spectroscopic techniques (Raman, infrared and energy-dispersive X-ray) as well as its morphology by scanning electron microscopy and compared to the analogously prepared reduced graphene oxide (rGO) and ruthenium oxide hexacyanoferrate (RuOHCF) thin films spectra and images. The results suggest that the improvement of the nanocomposite electrochemical activity is generated by the well-distributed RuOHCF nanometric particles over high-surfaced graphene sheets. Ethanol electrochemical oxidation in the rGO/RuOHCF modified electrode was performed in 0.1 mol L^{-1} NaCl (pH = 1.5) solution and it showed an anodic current peak starting at 0.9 V. Scan rate tests exhibited a diffusion-controlled process not followed by any coupled chemical reaction. The determination of ethanol by amperometry coupled with batch injection analysis (BIA) system resulted in a wide linear range (20-400 mmol L^{-1}) and good sensitivity (0.150 μA L mmol^{-1}). The nanocomposite also showed application as an electrochemical sensor of ethanol in commercial samples mainly because of its easy preparation comparing to biosensors.

Keywords: ruthenium Prussian Blue analogue, carbon nanomaterial, hexacyanoferrate particles, batch injection analysis

Introduction

The development of ethanol sensors must be accurate and sensitive due to its utility in many different areas. Forensic and medical fields require this substance quantity measurement for many kinds of biological samples as urine, blood, sweat, and others.[1-4] Nowadays, due to the coronavirus disease 2019 (COVID-19) pandemic, the use of ethanol as a general-purpose disinfectant has increased on a large scale, so it is very important to attest the quality of the product. Besides these, agricultural, environmental and food industries need quick and precise analysis methods for ethanol monitoring in diverse aqueous samples.[5-7] Since 1975, Brazil motivates ethanol production based on the fermentation and distillation of sugarcane juice for its utilization as an alternative fuel in its anhydrous form or diluted in gasoline matrix and also in beverage production, principally for a highly consumed liquor based on sugarcane called cachaça.[8,9]

The ethylic alcohol concentration can be evaluated by various methods such as mass spectroscopy,[10] liquid chromatography,[11] gas chromatography,[12] refractometry,[13] Raman spectroscopy,[14] nuclear magnetic resonance,[15] and electrochemistry.[16,17] The latter technique, comparing to the others, shows a lower cost and simplified instrumentation[18,19] which are desirable characteristics for ethanol content analysis mainly in simpler matrixes such as commercial alcohol and distilled drinks. Furthermore, the sensitivity, speed, and reagent savings can be easily improved by using the batch injection analysis (BIA) system.[20,21] This accessory was developed by Wang and Taha[22] based on flow injection analysis systems without the use of pipes and valves, which eliminates issues caused by bubbles or flow obstructions.[23] The procedure consists of the injection of small volumes of sample close and directly on the electrode surface, which is immersed in a great amount of supporting electrolyte. This scheme is called wall-jet. Its hydrodynamics fundaments combined to the huge dilution of the sample are the key of the BIA systems remarkable attributes.[24] Moreover, the instrumentation set provides the possibility to run on-site analysis when coupled to a portable potentiostat.[25]

The electroanalytical field provides the possibility of using various materials in the electrode surface enhancing

*e-mail: enossol@ufu.br

the sensitivity and stability supported by adequate selectivity. Graphene, a two-dimensional structure of sp^2 carbon atoms, is a promising option as a modifier agent mainly because of its high surface area and electrical conductivity.[26] For electroanalytical measurements these properties favor the charge transfer although in primitive graphene the electrocatalytic activity is not so prominent. An alternative to solve that problem is to use a derivative of graphene with functional oxygen groups in its framework.[27] This material, called graphene oxide (GO), is hydrophilic because of the presence of oxygen grouping, generating defects that are highly reactive sites and can promote the electrocatalysis of several chemical species.[28,29] The high amount of defects can harm the electron transfer, so it is important to produce a structure with very significant sp^2 carbon atoms. This procedure can be performed by reducing GO, and it can be made by some techniques such as electrochemical,[30] chemical,[31] or thermal[32] routes. The former technique, in contrast to the others, shows simplicity, quickness, lower-cost and toxic reactants-free. The electrochemical reduction of GO can be performed by the application of an appropriate potential in an aqueous GO dispersion to control the procedure, eliminating the oxygen functional groups and depositing a solid and conductive material in the working electrode surface.[30] Another advantage of using this method is the possibility to reduce other species simultaneously, generating nanocomposites and improving its electrocatalytic properties for analytical purposes.[33,34] Anyway, graphene-based composites are largely used materials for determination of several kinds of chemical species.[35-39]

The Prussian Blue analogues are face-centered cubic structured compounds with multivalent metal sites octaedrically coordinated by cyano groups which general formula can be demonstrated by $A_aM_m[M'_n(CN)_6].kH_2O$, where a, m, n, and k are stoichiometric numbers, M and M' are transition metals and A is, generally, an alkali metal ion.[40] These compounds are abundantly used in electrocatalysis as electrochemical sensors mainly because of their stability and reversibility.[41,42] As well as reduced graphene oxide, metal hexacyanoferrates can be produced by electrochemical method applying adequate electrical potential in the presence of potassium ferricyanide and a metal salt.[41] Particularly, the ruthenium oxide hexacyanoferrate is an excellent electrocatalyst material because of its wide active potential range and it is capable to mediate oxidation and/or reduction of several kinds of species.[43-45] Moreover, in that Prussian Blue analogue, oxygen atoms are acting as bridges in the structure, promoting an enhancement in electrochemical stability[45] and complementing a set of ideal properties for modifying

agents in electrode surfaces. After all, these characteristics can, even more, be upgraded if metal hexacyanoferrate nanoparticles are produced over highly conductive graphene sheets with a large surface area.[46]

The aiming of this work is to produce a nanocomposite based on reduced graphene oxide decorated with ruthenium oxide hexacyanoferrate (rGO/RuOHCF) using a two-step electrochemical approach. The material of interest is compared with its isolated components by several characterization methods for better elucidation of its composition. Furthermore, the nanocomposite electrocatalytic activity is tested for ethanol oxidation by amperometry using the convenient BIA system, which enables the composition prediction of the analyte in commercial samples.

Experimental

Chemicals

All the solutions and dispersions were prepared using deionized water (resistivity ≥ 18 MΩ cm) obtained in a Milli-Q water purification system (Millipore, Bedford, Massachusetts, USA). Ruthenium chloride, chloride acid, and sodium phosphate dibasic were acquired from Sigma-Aldrich (St. Louis, Missouri, USA) and graphite oxide (90%, m/m) from CN Shanghai (Shanghai, China). Sodium hydroxide (97%, m/m) was purchased from Quimex (São Paulo, São Paulo, Brazil) and potassium ferricyanide (99%, m/m) from Panreac (Castellar del Vallès, Barcelona, Spain). Sodium chloride (99%, m/m) was obtained from Vetec (São Paulo, São Paulo, Brazil) as well as phosphoric acid (85%, v/v), and ethanol (99.8%, v/v) was obtained from Synth (Diadema, São Paulo, Brazil).

Instrumentation

Electrochemical measurements were controlled through NOVA 2.1 software in a microcomputer connected to an AutoLab PGSTAT 12 potentiostat/galvanostat (Metrohm AutoLab B. V., Utrecht, Netherlands). As counter electrode, it was used a platinum wire and as reference electrode, an $Ag_{(s)}/AgCl_{(s)}/Cl^-_{(aq)}$ (KCl 3 mol L^{-1}) lab-made micro-electrode.[47] The material was synthesized over a working glassy carbon electrode (GCE) for electrochemical measurements and over a fluorine-doped tin oxide (FTO) glass for characterization techniques.

Raman spectroscopy was performed in a LabRAM HR Evolution microscope (HORIBA, Kyoto, Japan) using a 633 nm argon ion laser with 10% incidence potency. The Fourier transform infrared (FTIR) spectra were obtained

by a Frontier MIR/FIR from PerkinElmer (Waltham, USA) coupled to a diamond-equipped attenuated total reflectance (ATR) accessory from Pike Technologies (Madison, USA). Thin films images were acquired by scanning electron microscopy (SEM) on a Vega 3 microscope (Tescan, Czech Republic) operated at 20 kV and elemental analysis were obtained by energy-dispersive X-ray spectroscopy (EDX) technique using an INCA X-Act (Oxford Instruments, Abingdon, UK) detector. The particle size on nanocomposite was estimated by the measurement of 100 nanoparticles utilizing the ImageJ software.[48]

Thin films synthesis

The treatment of glassy carbon electrode was made by polishing the surface in an alumina power (0.3 μm) suspension followed by a deionized water rinsing and then put in water/ethanol (1:1) solution for 5 min sonication.

The rGO/RuOHCF nanocomposite was entirely fabricated by the cyclic voltammetry (CV) method. The first step consists in the three-electrode system immersed in a 10-min sonicated 10 mL dispersion (pH = 3.0) containing 0.1 mg mL^{-1} graphene oxide, 1.0 mmol L^{-1} RuCl$_3$ and 0.05 mol L^{-1} Na$_2$HPO$_4$ as supporting electrolyte and then 10 voltammetric cycles, at 20 mV s^{-1}, from 0 to −1.5 V were applied for rGO/RuO$_x$ precursor deposition. Secondly, after dried at room temperature, this modified electrode was submitted to 8 voltammetric cycles, at 100 mV s^{-1}, from −0.3 to 1.3 V in a solution (pH = 1.5) containing 0.1 mol L^{-1} NaCl and 1.0 mmol L^{-1} K$_3$[Fe(CN)$_6$] for nanoparticle composition modification. The pH was adjusted using a concentrated H$_3$PO$_4$ solution for the first step while for the second step a concentrated HCl solution was used. These acidic species were chosen to alter pH keeping the same anion from the supporting electrolyte in the composition of the solutions.

The rGO thin film was obtained the same way as rGO/RuOHCF nanocomposite, however, in the absence of RuCl$_3$, whereas the RuOHCF thin film preparation was in absence of GO precursor. The preparation of all materials was made at room temperature and in the presence of oxygen.

Ethanol electrochemical determination

The determination of ethanol based on its electrochemical oxidation in rGO/RuOHCF modified electrode was performed by amperometry technique coupled to a batch injection analysis system. The BIA cell was constituted by a 200 mL capacity cylindrical glass and it has a top cover with holes on the edges for a mechanical stirrer and for reference and counter electrodes. At the center of the same cover, there is an orifice for a micropipette tip accommodation at 2 mm distanced of the working electrode, which is accommodated in the bottom cover.[49] This configuration generates current peak signals that are proportional to the analyte concentration and it is known as "wall-jet".[22]

The rGO/RuOHCF modified electrode was prepared using 20 voltammetric cycles in 0.1 mol L^{-1} NaCl (pH = 1.5) for current stabilization before all measurements. No buffer was needed due to high difference between analyte and supporting electrolyte concentrations, once EtOH is incapable to variate this pH magnitude. The analytical curve was obtained by the injection of prepared ethanol solutions with well-known concentrations in the supporting electrolyte. The injections in the BIA cell were performed with an Eppendorf Multipette® stream electronic pipette attached to a Multipette® Combitip®. A previous optimization of the applied potential (0.8, 0.9, 1.0, 1.1, and 1.2 V), dispensing speed (78.1, 164.0, 213.0, 277.0, and 370.0 μL s^{-1}), and dispensing volume (20, 40, 60, 80, and 100 μL) were carried out by fixing two of the three parameters at the median value and collecting the response of the current peak with the highest intensity and lowest relative standard deviation (RSD). The commercial alcohol and cachaça samples were simply diluted in supporting electrolyte containing 50.0 mmol L^{-1} of standard ethanol and were injected at the end of the analytical curve. All the BIA measurements were performed under mechanical stirring.

Results and Discussion

rGO/RuOHCF nanocomposite synthesis

The preparation of the rGO/RuOHCF nanocomposite was performed in two steps but using the same technique. A 10-cycles voltammetry, at 20 mV s^{-1}, from 0 to −1.5 V was applied on the three-electrode system immersed in the GO dispersion (pH = 3) containing the ruthenium chloride as nanoparticle source and the supporting electrolyte under magnetic stirring. This first step, shown in Figure 1a, generated a voltammogram with an irreversible cathodic peak which is related to the reduction of GO, while the relative increase in each cycle can be associated with the quantity of conductor material depositing in the working electrode surface.[50] The acid media, although it stimulates the hydrogen evolution around −1.5 V, promotes the protonation of the oxygen-containing groups of GO, which plays an important role on the reduction process kinetics.[51] So the constant stirring during the electrodeposition helps removing generated hydrogen gas bubbles competing for

sites on the electrode surface.[52] Also a cathodic peak at -0.5 V is perceived, which is related to the reduction of Ru^{3+} to metallic and oxy-chloro ruthenium species that, in the successive scans, are converted to hydroxyl and/or oxy-abundant Ru species.[53] The low pH of the dispersion avoids previous precipitation of ruthenium hydroxide and keeps the Ru^{3+} available for the electrochemical reduction.[54]

The product of the first step, a nanocomposite containing rGO and ruthenium oxide species, was dried at room temperature and submitted to a second procedure. This step consists of the immersion of the previously modified electrode in a solution (pH = 1.5) containing potassium ferricyanide and sodium chloride as supporting electrolyte for nanoparticle structural modification. The low pH level was chosen to increase the dissociation of ferricyanide, resulting in faster nucleation kinetics, and as consequence to increase the formation of RuOHCF.[55,56] Moreover, at higher electrochemical potentials and more acidic media the stripping of ruthenium nanoparticles is favored.[57] From -0.3 to 1.3 V, 8 scans at 100 mV s^{-1} are performed for the desirable nanocomposite fabrication which voltammogram can be checked in Figure 1b. A reaction between the oxide nanoparticles and ferricyanide happens in the first scans forming the RuOHCF nanoparticles. The saturation of these species is reached in the final scans, generating a typical electrochemical profile of the Prussian Blue analogue with characteristic redox pairs.[43]

Electrochemical studies

The electrochemical profile between 0.3 and 1.25 V of the rGO/RuOHCF nanocomposite was compared to analogously prepared rGO and RuOHCF thin films and it is shown in Figure 2a. The isolated RuOHCF film shows three well-defined redox pairs which are assigned to ruthenium and iron electron transfer processes: at -0.05 V the reaction is related to $Ru^{II}O[Fe^{II}(CN)_6]/Ru^{III}O[Fe^{II}(CN)_6]$, at 0.9 V is related to $Ru^{III}O[Fe^{III}(CN)_6]/Ru^{IV}O[Fe^{III}(CN)_6]$ and at 1.1 V

is related to $Ru^{IV}O[Fe^{III}(CN)_6]/Ru^{VI}O[Fe^{III}(CN)_6]$.[46] The system electroneutrality is established by the diffusion of sodium ion in the framework. The rGO cyclic voltammogram shows a pseudo-capacitive behavior with a redox pair at 0.3 V attributed to functional oxygen groups that are too stable for elimination by the electrochemical method.[50] The presence of the characteristic redox pairs joining the increase of current intensity suggests the successful attachment of the RuOHCF nanoparticles to ample-area graphene sheets forming a nanocomposite with high synergic action.

RGO/RuOHCF and RuOHCF films had their stability tested in 0.1 mol L^{-1} NaCl supporting electrolyte with pH of 1.5, 4.0, 7.0, and 9.0 between -0.3 and 1.25 V. Figures 2b and 2c show the decrease of the relative current of the anodic peak at 1.1 V during 50 scans of RuOHCF and rGO/RuOHCF, respectively, and it demonstrates that the nanocomposite owns better stability in all pH values. This effect can be explained by the reduced graphene oxide supporting structure that, in addition to offering an increase of surface area and better electron transferring, it promotes more effectiveness of the Prussian Blue analogue nanoparticles attachment.[58] The lower pH value showed better stability during the cycles since higher pH values favor the precipitation of the ruthenium in its hydroxide form.[54] Therefore, the pH of 1.5 was chosen to be used in the next stages of the work.

Characterization

The three different materials, rGO, RuOHCF, and rGO/RuOHCF were submitted to a 633 nm argon ion laser to acquire Raman spectra that are shown in Figure 3a. For the RuOHCF, the typical C≡N stretching of the Prussian Blue analogues[59] appears at 2137 cm^{-1} and it is also present in the nanocomposite spectrum. Materials based on reduced graphene oxide have two main characteristic signals: the D and G bands. The former, around 1348 cm^{-1}, is related to defects on the sp^2 network generated during oxidation/
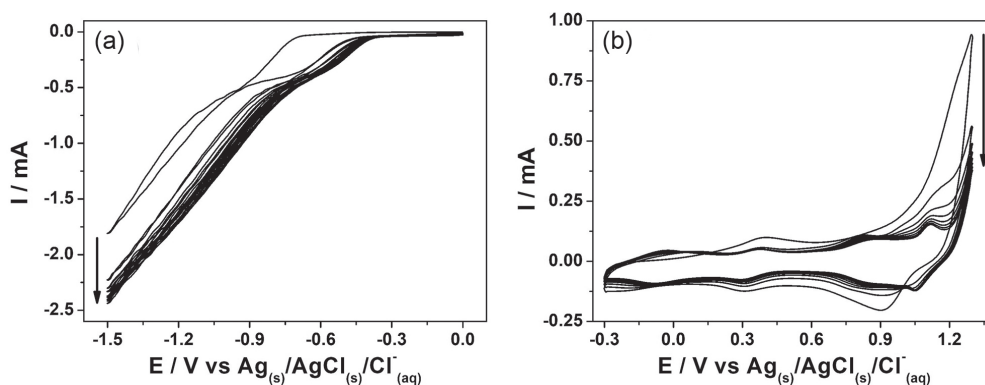

Figure 1. (a) Simultaneous electrochemical reduction of GO and Ru^{3+}; (b) rGO/RuOHCF film formation.

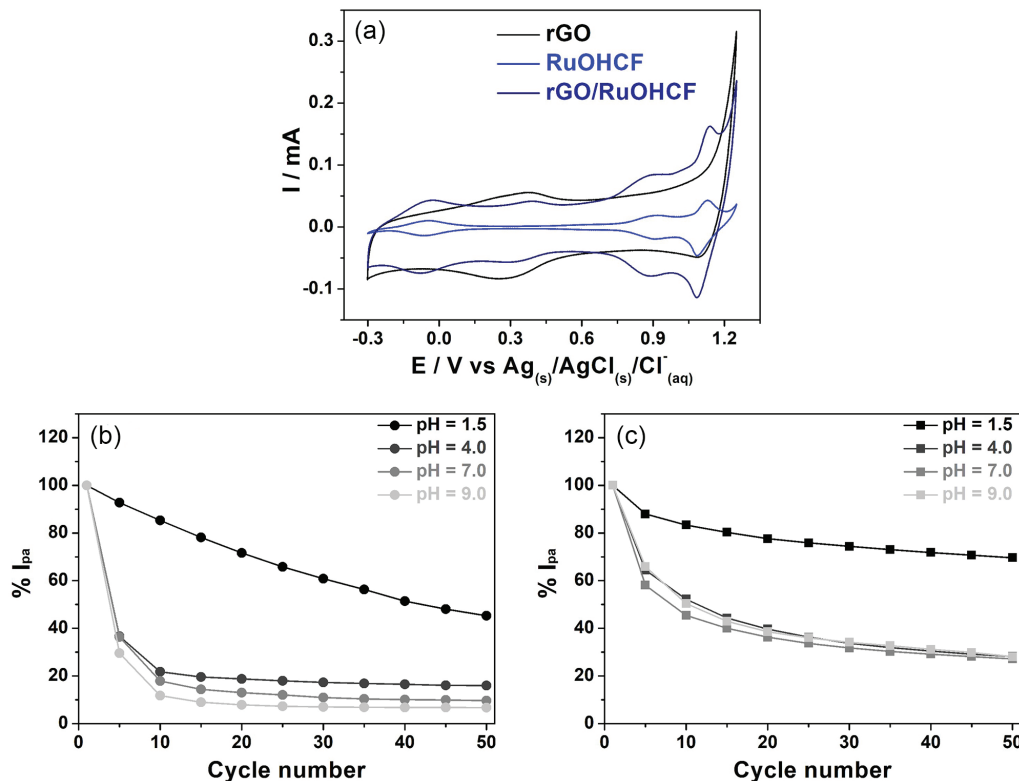**Figure 2.** (a) Electrochemical profile of the thin films in 0.1 mol L^{-1} NaCl (pH = 1.5); electrochemical stability for 50 scans in 0.1 mol L^{-1} NaCl of (b) RuOHCF and (c) rGO/RuOHCF.

reduction synthesis of the material, while the latter, around 1584 cm^{-1}, is associated with first-order scattering of the E$_{2g}$ symmetry and represents the in-plane vibration of the sp^2 carbon bonds.[60] The ratio between the area of the D and G bands (I$_D$/I$_G$) informs the degree of defects of the carbonaceous structures, presenting a value of 3.2 for rGO and 2.4 for rGO/RuOHCF films spectra. The decrease of the ratio in the nanocomposite indicates the reconstitution of the sp^2 carbon sites in the presence of the simultaneously-reduced nanoparticles.[61,62] The concurrent appearance of all the discussed bands in the Raman spectrum of the rGO/RuOHCF attest to the successful formation of the nanocomposite material.

Figure 3b shows the FTIR spectra for all the obtained films. The sharp band related to the cyanide group[63] stretching mode appears at 2070 cm^{-1} in the RuOHCF film spectrum which is also present in the nanocomposite film spectrum. The rGO spectrum exhibits, around 1550 cm^{-1}, a band associated with the C=C bond of the structural framework. Besides that, some bands related to the functional oxygen groups derived from the oxidation of the graphite is also shown, such as C–O (at 1370 and 1430 cm^{-1}) and C=O stretching (at 1645 and 1705 cm^{-1}).[64] All discussed bands can be perceived in the rGO/RuOHCF spectrum, which suggests the presence of the two materials in the same structure, composing the nanocomposite framework.
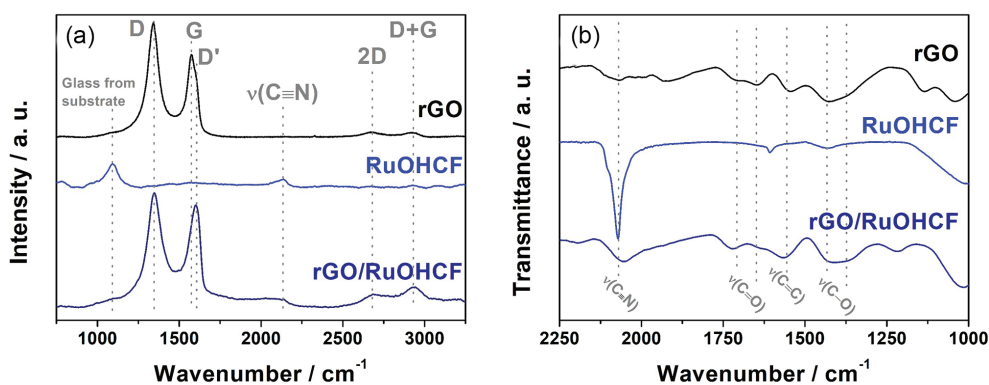

Figure 3. (a) Raman and (b) infrared (ATR) spectra of the thin films.

Surface morphology studies were made through SEM images and it is shown in Figure 4. rGO film exhibited wrinkled sheet-like morphology caused by defects and functional groups on its two-dimensional structure and this roughness implies a sharp increase of surface area.[65] Isolated-prepared RuOHCF film showed several nanoparticles that trend to form agglomerates micrometric-scaled. This effect does not happen in the rGO/RuOHCF nanocomposite, since the carbonaceous material acts as a nucleation center preventing the grown of the particles and keeping them well-dispersed over graphene sheets.[66] The size of the RuOHCF nanoparticles in the rGO/RuOHCF film was estimated to 89.3 nm on average.

The elemental composition of the films was analyzed by EDX and the spectra are shown in Figure 5. All of them had the presence of Sn and Si, which constitutes the structure of the FTO substrate. Sodium and phosphorous also appeared on the spectra and they have remained from the supporting electrolyte of the first step of the synthesis. rGO film showed the expected abundant C signal and the O signal from the functional oxygen groups. RuOHCF film exhibited a lower C signal because of the absence of the carbonaceous material and it has the same intensity of N signal, which constitutes the cyanide ligand from the Prussian Blue analogue structure. The presence of Ru and
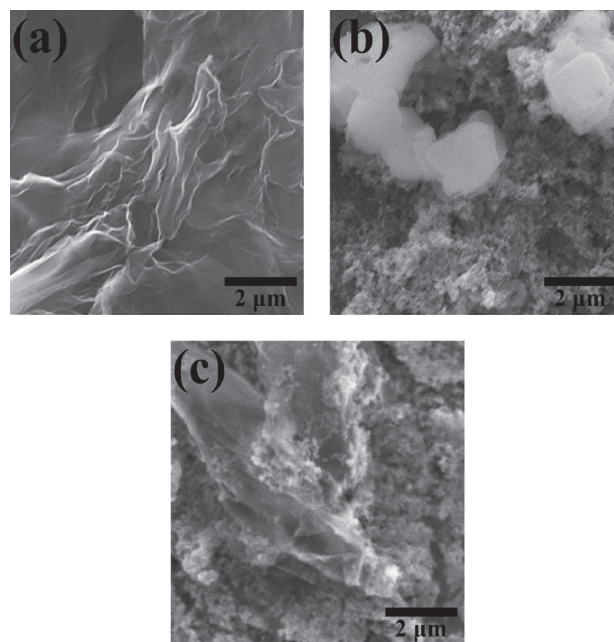

Figure 4. SEM images of (a) rGO, (b) RuOHCF, and (c) rGO/RuOHCF thin films.

Fe signals are also shown as well as in the rGO/RuOHCF spectrum. The rise of the C signal in the rGO/RuOHCF spectrum and the appearance of the signals mentioned above suggests the presence of the carbon framework supporting the well-dispersed nanoparticles.
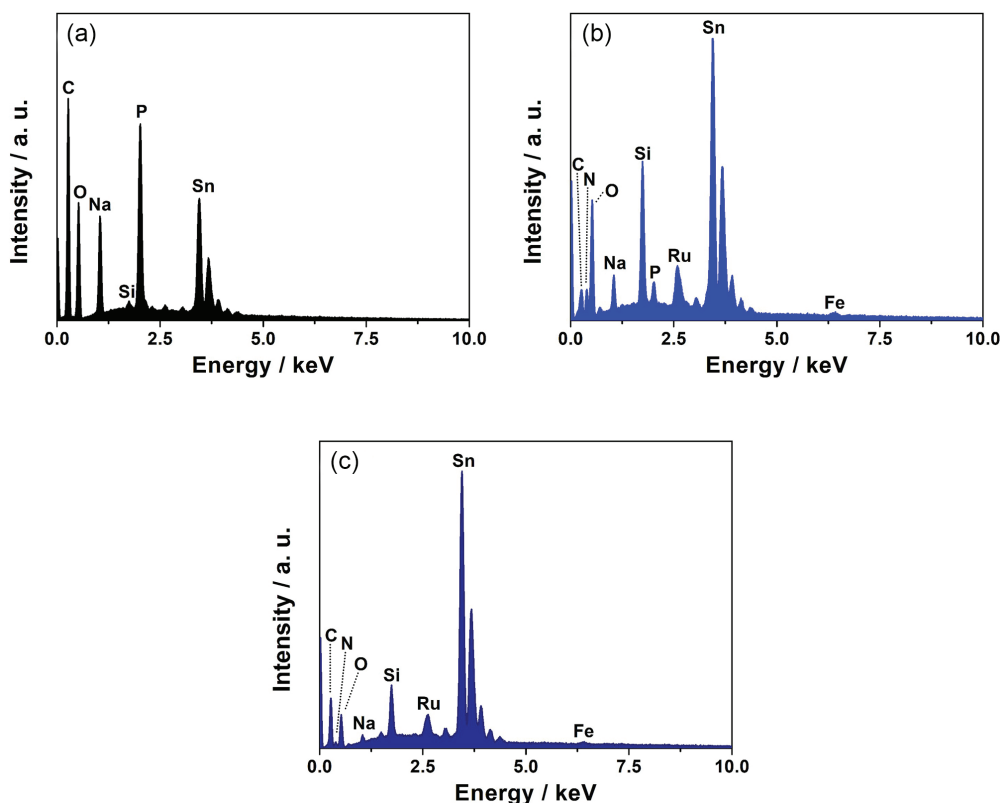

Figure 5. EDX spectra of (a) rGO, (b) RuOHCF and (c) rGO/RuOHCF thin films.

Ethanol electrochemical determination

The electrochemical behavior of ethanol in the rGO/RuOHCF modified electrode was studied in the optimized media discussed previously. A supporting electrolyte of 0.1 mol L^{-1} NaCl (pH = 1.5) was used for all electrochemical tests for ethanol electro-oxidation. The voltammetric profiles of the analyte on the modified and glassy carbon electrodes are shown in Figure 6a and attest an increase of anodic current starting at 0.9 V for rGO/RuOHCF, which corresponds to the electrochemical-stimulated oxidation of ethanol. The glassy carbon electrode did not present activity for ethanol oxidation in this range of potential. The reaction mediated by the Prussian Blue analogue part of the nanocomposite can be proposed by equation 1:[46,67]

$$rGO/Ru^{VI}O[Fe(CN)_6] + CH_3CH_2OH \rightarrow$$
$$rGO/Ru^{IV}O[Fe(CN)_6] + CH_3CHO + 2H^+ + 2e^- \quad (1)$$
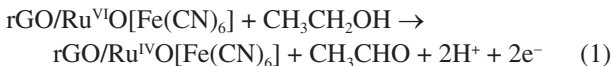
The behavior of the electrochemical reaction was also studied by scan rate test between 25 and 300 mV s^{-1}, and the voltammograms are shown in Figure 6b. The intensity of the anodic peak current around 1.1 V increases linearly with the increasing of the square of the scan rate (Figure 6c), which implies in a diffusion-controlled process.[68] The reaction is not followed by any coupled chemical reaction, being purely diffusional, which is proven by the near 0.5 slope value of the logarithmic relationship between the variables (Figure 6d).[69]

The determination of ethanol was performed by amperometry assisted with BIA system. The applied potential, dispensing rate, and dispensing volume were optimized and the chosen values were 1.1 V, 213.0 μL s^{-1} and 80 μL, respectively. Under mechanical stirring, the analytical curves of increasing and decreasing ethanol concentrations were constructed by the injection of the standard analyte (Figure 7a) while the commercial samples were injected between the curves (A and C signals). The amperogram of the injections from 20.0 to 400.0 mmol L^{-1} of standard ethanol increases according to the sequential additions and the calibration curves present good linear correlation (R > 0.98) as can be checked in the inset of Figure 7a. Figure 7b shows the repeatability test for low (20 mmol L^{-1}) and high concentration (240 mmol L^{-1}) solutions of ethanol and the obtained RSD values were 7 and 11%, respectively. The limits of detection (LOD) and quantification (LOQ) were calculated by $3S_b/S$ and $10S_b/S$ (where S_b is the RSD of 10-times measured blank solution and S is the slope of the curve), respectively.[70]

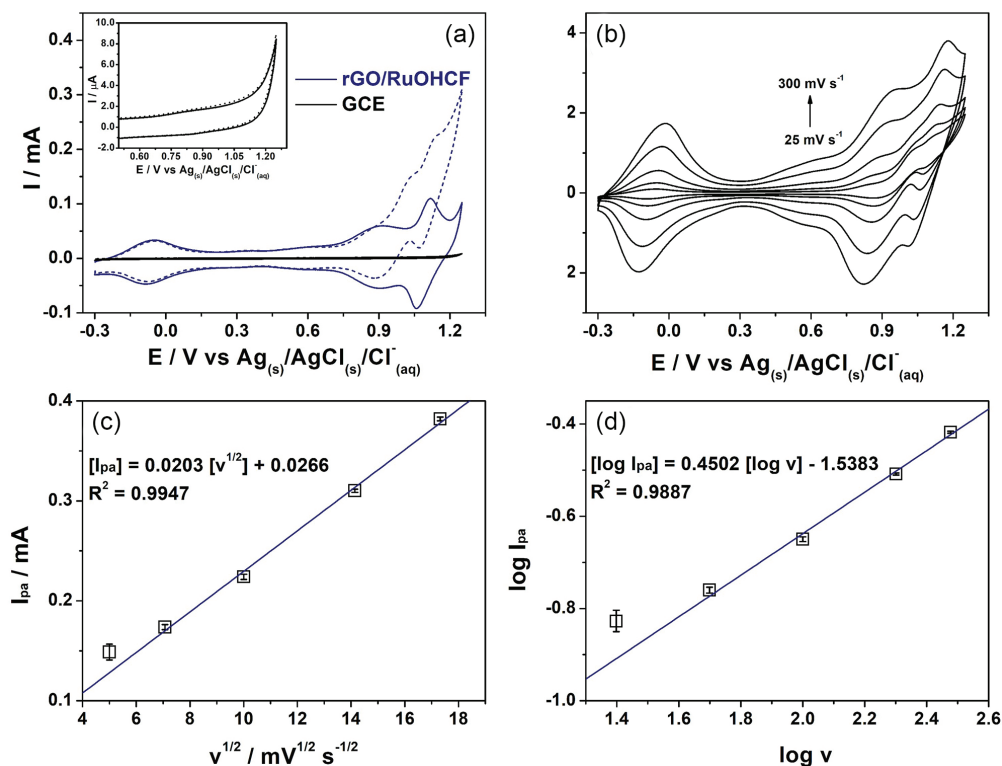The selectivity, reproducibility, and stability of rGO/RuOHCF modified electrode was also tested by

Figure 6. (a) rGO/RuOHCF and GCE (inset) voltammetric behavior (0.1 mol L^{-1} NaCl, pH = 1.5) in 150 mmol L^{-1} of ethanol (dashed line) and support electrolyte (solid line) solutions; (b) scan rate test (25, 50, 100, 200, and 300 mV s^{-1}) voltammetry of rGO/RuOHCF modified electrode in the presence of 150 mmol L^{-1} of ethanol in 0.1 mol L^{-1} NaCl; (c) I_{pa} versus $v^{1/2}$ and (d) log I_{pa} versus log v plots.
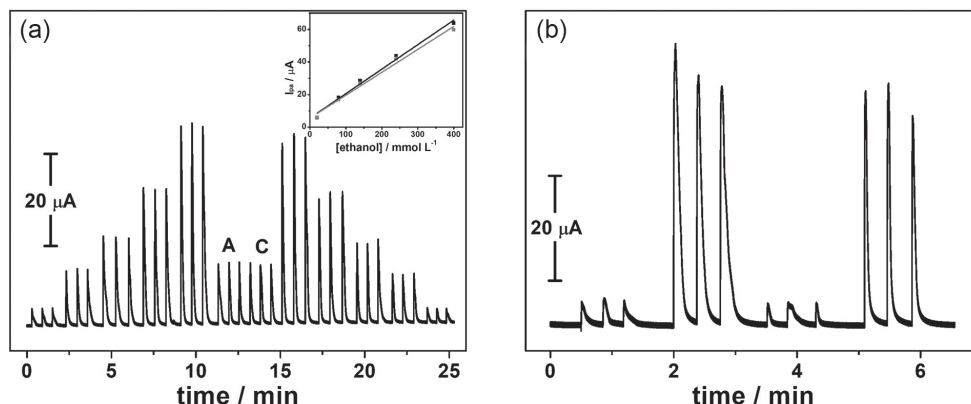
Figure 7. (a) Ethanol BIA/amperometric determination (from 20.0 to 400.0 mmol L^{-1}) and calibration plots (inset), and (b) repeatability test by BIA/amperometry in 0.1 mol L^{-1} NaCl by rGO/RuOHCF modified electrode. Applied potential: 1.1 V; dispensing rate: 213.0 μL s^{-1}; dispensing volume: 80 μL.

BIA/amperometry under the same conditions. Figure 8a shows the response of four species that could be present in the EtOH fermentation process. The alcohols showed intense peaks, which was expected based on previous works.[44,71] All species were injected for 3-fold excess, so: methanol showed 89.3% of EtOH relative current, isopropanol and *n*-butanol exhibited 378.7 and 384.1%, respectively, while glucose showed only 28.1%. In summary, all other species undergo oxidation processes on the modified electrode, so they can be considered interferents, especially isopropanol and *n*-butanol.

Three rGO/RuOHCF modified electrodes were prepared to evaluate its reproducibility. Figure 8b shows a low peak current difference between them, proving the method of electrode preparation is easily replicable. Also, the material stability was evaluated (Figure 8c) showing good results. It exhibited, on the second day, a slight increase of 11% of relative current compared to day one, while day three the current intensity keeps practically the same than the day before, proving the rGO/RuOHCF modified electrode can be stored for 3 days without losing electroanalytical efficiency.
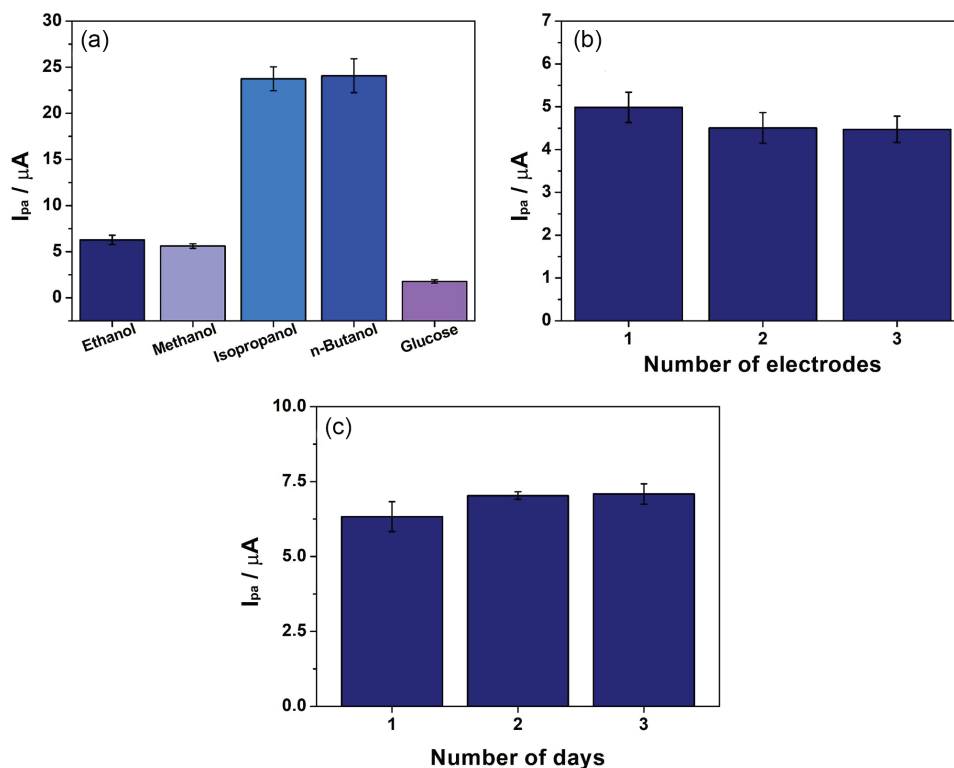

Figure 8. BIA/amperometric results of rGO/RuOHCF modified electrode under injection of 20 μmol L^{-1} EtOH and 60 μmol L^{-1} (3-fold) interfering species (n = 3) (a). Response of three different rGO/RuOHCF modified electrodes (20 μmol L^{-1} EtOH) (b). Stability response of rGO/RuOHCF modified electrode for three days (20 μmol L^{-1} EtOH) (c). Supporting electrolyte: 0.1 mol L^{-1} NaCl (pH = 1.5); applied potential: 1.1 V; dispensing rate: 213.0 μL s^{-1}; dispensing volume: 80 μL.

Table 1. Electroanalytical parameters of ethanol determination by amperometry of several materials

Material	Linear range / (mmol L^{-1})	Sensitivity / (µA mmol L^{-1})	LOD / (mmol L^{-1})	LOQ / (mmol L^{-1})	Reference
Gr/Pd-NP	2.0-210.0	–	2.0	–	72
PDDA-[CG-AOx]$_5$	0.25-1.5	0.032	0.05	–	73
ADH/HRP	10.0-80.0	–	2.85	9.50	74
RuHCF	30-400	0.21	0.76		67
MWCNT/RuHCF	0.2-1.7	1,3	0.1	–	71
rGO/RuOHCF	5.0-400.0	0.150	0.50	1.68	this work

LOD: limit of detection; LOQ: limit of quantification; Gr/Pd-NP: graphene/palladium nanoparticles; PDDA-[CG-AOx]$_5$: poly diallyldimethylammonium chloride-[carboxylated graphene-alcohol oxidase]; ADH/HRP: alcohol dehydrogenase/horseradish peroxidase; RuHCF: ruthenium hexacyanoferrate; MWCNT/RuHCF: multiwalled carbon nanotubes/ruthenium hexacyanoferrate; rGO/RuOHCF: reduced graphene oxide/ruthenium oxide hexacyanoferrate.

Table 1 presents the electroanalytical parameters obtained by various materials in literature[67,71-74] including this work, which the compared values presented good results, especially regarding the wide linear range. Specifically, when the material prepared in this work is compared with the other ruthenium hexacyanoferrates based sensors presented in Table 1, it became clear that the proposed method results in a higher covering of the substrate by the hexacyanoferrate, with possibility of detection ethanol in a wide concentration range. Moreover, the electrode showed good reproducibility and stability, since this type of study was not explored by the papers mentioned above.[67,71-74] The facility of the electrode material preparation in contrast to biosensors is also a point to be considered.

The commercial samples analysis of hydrated pharmacy alcohol and cachaça applying the rGO/RuOHCF modified electrode, using the BIA/amperometry method, showed good agreement with the labeled content by the fabricants for both samples. The converted values obtained for hydrated alcohol (A) and cachaça (C) samples injected (see Figure 7a) are exhibited in Table 2. The unity of the hydrated alcohol is shown as °INPM, which is the unity used for this substance in Brazil. It means Instituto Nacional de Pesos e Medidas (National Institute of Weights and Measurements) and constitutes the quantity of absolute ethanol in each 100 g of hydro-alcoholic solution.

Table 2. Concentrations of ethanol found in commercial samples obtained by BIA/amperometry using the rGO/RuOHCF modified electrode and respective relative standard deviations (n = 3)

Sample	Labeled	Found
Alcohol (A) / °INPM	46	45 ± 1
Cachaça (C) / % (v/v)	39	36 ± 1

°INPM: Instituto Nacional de Pesos e Medidas degree.

Conclusions

This work demonstrated an easy method for the fabrication of reduced graphene oxide/ruthenium oxide hexacyanoferrate nanocomposite material for direct electrode modification. The characterization methods showed the morphological and structural characteristics of the material that acts as a promising material for ethanol electrochemical determination. The electroanalytical results exhibited ample linear range in acidic media using amperometry coupled with a batch injection analysis system. The rGO/RuOHCF modified electrode was successfully tested for ethanol commercial samples demonstrating less than 10% variation related to labeled by the product fabricators.

Acknowledgments

References

1. de Martinis, B. S.; Ruzzene, M. A. M.; Martin, C. C. S.; *Anal. Chim. Acta* **2004**, *522*, 163.

2. Arakawa, T.; Suzuki, T.; Tsujii, M.; Iitani, K.; Chien, P.-J.; Ye, M.; Toma, K.; Iwasaki, Y.; Mitsubayashi, K.; *Biosens. Bioelectron.* **2019**, *129*, 245.

3. Bueno, L. H. P.; da Silva, R. H. A.; Azenha, A. V.; Dias, M. C. S.; de Martinis, B. S.; *Forensic Sci. Int.* **2014**, *242*, 117.

4. Gamella, M.; Campuzano, S.; Manso, J.; de Rivera, G. G.; López-Colino, F.; Reviejo, A. J.; Pingarrón, J. M.; *Anal. Chim. Acta* **2014**, *806*, 1.

5. Huida, L.; *Agric. Food Sci.* **1982**, *54*, 137.

6. Prasad, P. R.; Rama Rao, K. S.; Bhuvaneswari, K.; Praveena, N.; Srikanth, Y. V. V.; *Energy Sources, Part A* **2008**, *30*, 1534.

7. Sisco, E.; Robinson, E. L.; *Forensic Chem.* **2020**, *18*, 100219.

8. Guerra, J. B.; Araújo, R. A. C.; Pataro, C.; Franco, G. R.; Moreira, E. S. A.; Mendonça-Hagler, L. C.; Rosa, C. A.; *Lett. Appl. Microbiol.* **2001**, *33*, 106.

9. Martinelli, L. A.; Filoso, S.; *Ecol. Appl.* **2008**, *18*, 885.

10. Jones, A. W.; Mårdh, G.; Änggård, E.; *Pharmacol., Biochem. Behav.* **1983**, *18*, 267.

11. López, E. F.; Gómez, E. F.; *J. Chromatogr. Sci.* **1996**, *34*, 254.

12. Pontes, H.; de Pinho, P. G.; Casal, S.; Carmo, H.; Santos, A.; Magalhães, T.; Remião, F.; Carvalho, F.; Bastos, M. L.; *J. Chromatogr. Sci.* **2009**, *47*, 272.

13. Owuama, C. I.; Ododo, J. C.; *Food Chem.* **1993**, *48*, 415.

14. Sanford, C. L.; Mantooth, B. A.; Jones, B. T.; *J. Chem. Educ.* **2001**, *78*, 1221.

15. Zuriarrain, A.; Zuriarrain, J.; Villar, M.; Berregi, I.; *Food Control* **2015**, *50*, 758.

16. Shan, C.; Yang, H.; Han, D.; Zhang, Q.; Ivaska, A.; Niu, L.; *Biosens. Bioelectron.* **2010**, *25*, 1504.

17. Huang, H.-Y.; Chen, P.-Y.; *Talanta* **2010**, *83*, 379.

18. Nasirizadeh, N.; Ghaani, M.; Shekari, Z.; Shateri-Khalilabad, M.; *J. Braz. Chem. Soc.* **2016**, *27*, 1577.

19. Veloso, W. B.; Ribeiro, G. A. C.; da Rocha, C. Q.; Tanaka, A. A.; da Silva, I. S.; Dantas, L. M. F.; *Measurement* **2020**, *155*, 107516.

20. Rocha, D. P.; Cardoso, R. M.; Tormin, T. F.; de Araujo, W. R.; Munoz, R. A. A.; Richter, E. M.; Angnes, L.; *Electroanalysis* **2018**, *30*, 1386.

21. Ribeiro, G. A. C.; da Rocha, C. Q.; Veloso, W. B.; Dantas, L. M. F.; Richter, E. M.; da Silva, I. S.; Tanaka, A. A.; *J. Solid State Electrochem.* **2020**, *24*, 1759.

22. Wang, J.; Taha, Z.; *Anal. Chem.* **1991**, *63*, 1053.

23. Cunha, R. R.; Tormin, T. F.; Richter, E. M.; Munoz, R. A. A.; *Quim. Nova* **2013**, *36*, 663.

24. Quintino, M. S. M.; Angnes, L.; *Electroanalysis* **2004**, *16*, 513.

25. Oliveira, T. C.; Santana, M. H. P.; Banks, C. E.; Munoz, R. A. A.; Richter, E. M.; *Electroanalysis* **2019**, *31*, 567.

26. Beitollai, H.; Safaei, M.; Tajik, S.; *Int. J. Nano Dimens.* **2019**, *10*, 125.

27. Guo, N.; Yam, K. M.; Zhang, C.; *npj 2D Mater. Appl.* **2018**, *2*, 1.

28. Ahmad, H.; Fan, M.; Hui, D.; *Composites, Part B* **2018**, *145*, 270.

29. Rowley-Neale, S. J.; Randviir, E. P.; Abo Dena, A. S.; Banks, C. E.; *Appl. Mater. Today* **2018**, *10*, 218.

30. Toh, S. Y.; Loh, K. S.; Kamarudin, S. K.; Daud, W. R. W.; *Chem. Eng. J.* **2014**, *251*, 422.

31. Chua, C. K.; Pumera, M.; *Chem. Soc. Rev.* **2014**, *43*, 291.

32. Chen, W.; Yan, L.; Bangal, P. R.; *Carbon* **2010**, *48*, 1146.

33. Moradi Golsheikh, A.; Huang, N. M.; Lim, H. N.; Zakaria, R.; Yin, C.-Y.; *Carbon* **2013**, *62*, 405.

34. Shi, R.; Liang, J.; Zhao, Z.; Liu, A.; Tian, Y.; *Talanta* **2017**, *169*, 37.

35. Zhou, N.; Li, J.; Chen, H.; Liao, C.; Chen, L.; *Analyst* **2013**, *138*, 1091.

36. Chen, D.; Zhuang, X.; Zhai, J.; Zheng, Y.; Lu, H.; Chen, L.; *Sens. Actuators, B* **2018**, *255*, 1500.

37. Zhuang, X.; Chen, D.; Zhang, S.; Luan, F.; Chen, L.; *Microchim. Acta* **2018**, *185*, 166.

38. Thirumalraj, B.; Rajkumar, C.; Chen, S.-M.; Veerakumar, P.; Perumal, P.; Liu, S.-B.; *Sens. Actuators, B* **2018**, *257*, 48.

39. Luan, F.; Zhang, S.; Chen, D.; Wei, F.; Zhuang, X.; *Microchem. J.* **2018**, *143*, 450.

40. Zhang, W.; Zhao, Y.; Malgras, V.; Ji, Q.; Jiang, D.; Qi, R.; Ariga, K.; Yamauchi, Y.; Liu, J.; Jiang, J.-S.; Hu, M.; *Angew. Chem., Int. Ed.* **2016**, *55*, 8228.

41. Karyakin, A. A.; *Curr. Opin. Electrochem.* **2017**, *5*, 92.

42. Karyakin, A. A.; Karyakina, E. E.; *Russ. Chem. Bull.* **2001**, *50*, 1811.

43. Kumar, A. S.; Zen, J.-M.; *Electroanalysis* **2004**, *16*, 1211.

44. Chen, S.-M.; Lu, M.-F.; Lin, K.-C.; *J. Electroanal. Chem.* **2005**, *579*, 163.

45. Shaidarova, L. G.; Ziganshina, S. A.; Tikhonova, L. N.; Budnikov, G. K.; *J. Anal. Chem.* **2003**, *58*, 1144.

46. Borges, P. H. S.; Catto, A. C.; Longo, E.; Nossol, E.; *J. Electroanal. Chem.* **2020**, *878*, 114558.

47. Pedrotti, J. J.; Angnes, L.; Gutz, I. G. R.; *Electroanalysis* **1996**, *8*, 673.

48. Rasband, W. S.; *ImageJ*, 1.53e; U. S. National Institutes of Health, Bethesda, Maryland, USA, 2020.

49. Silva, R. A. B.; Montes, R. H. O.; Richter, E. M.; Munoz, R. A. A.; *Food Chem.* **2012**, *133*, 200.

50. Chen, L.; Tang, Y.; Wang, K.; Liu, C.; Luo, S.; *Electrochem. Commun.* **2011**, *13*, 133.

51. Quezada-Renteria, J. A.; Ania, C. O.; Chazaro-Ruiz, L. F.; Rangel-Mendez, J. R.; *Carbon* **2019**, *149*, 722.

52. Guo, H.-L.; Wang, X.-F.; Qian, Q.-Y.; Wang, F.-B.; Xia, X.-H.; *ACS Nano* **2009**, *3*, 2653.

53. Li, M.; He, H.; *Appl. Surf. Sci.* **2018**, *439*, 612.

54. Raoof, J. B.; Ojani, R.; Baghayeri, M.; *Anal. Methods* **2011**, *3*, 2367.

55. Ding, Y.; Gu, G.; Xia, X.-H.; *J. Solid State Electrochem.* **2008**, *12*, 553.

56. Neale, Z. G.; Liu, C.; Cao, G.; *Sustainable Energy Fuels* **2020**, *4*, 2884.

57. Dattilo, D.; Dietze, U.; Hsu, J.-W.; *Proc. SPIE* **2015**, *9635*, 96351B.

58. Kim, J.-Y.; Kim, K.-H.; Yoon, S.-B.; Kim, H.-K.; Park, S.-H.; Kim, K.-B.; *Nanoscale* **2013**, *5*, 6804.

59. Gimenes, D. T.; Nossol, E.; *Electrochim. Acta* **2017**, *251*, 513.

60. Dresselhaus, M. S.; Jorio, A.; Hofmann, M.; Dresselhaus, G.; Saito, R.; *Nano Lett.* **2010**, *10*, 751.

61. How, G. T. S.; Pandikumar, A.; Ming, H. N.; Ngee, L. H.; *Sci. Rep.* **2014**, *4*, 5044.

62. Gigot, A.; Fontana, M.; Pirri, C. F.; Rivolo, P.; *Materials* **2018**, *11*, 57.

63. Pang, H.; Zhang, Y.; Cheng, T.; Lai, W.-Y.; Huang, W.; *Nanoscale* **2015**, *7*, 16012.

64. Ţucureanu, V.; Matei, A.; Avram, A. M.; *Crit. Rev. Anal. Chem.* **2016**, *46*, 502.

65. Eluyemi, M. S.; Eleruja, M. A.; Adedeji, A. V.; Olofinjana, B.; Fasakin, O.; Akinwunmi, O. O.; Ilori, O. O.; Famojuro, A. T.; Ayinde, S. A.; Ajayi, E. O. B.; *Graphene* **2016**, *5*, 143.

66. Singh, M. K.; Titus, E.; Krishna, R.; Hawaldar, R. R.; Goncalves, G.; Marques, P.; Gracio, J.; *J. Nanosci. Nanotechnol.* **2012**, *12*, 6731.

67. Costa, W. M.; Cardoso, W. S.; Marques, E. P.; Bezerra, C. W. B.; Ferreira, A. A. P.; Song, C.; Zhang, J.; Marques, A. L. B.; *J. Braz. Chem. Soc.* **2013**, *24*, 651.

68. Zhang, S.; Zhuang, X.; Chen, D.; Luan, F.; He, T.; Tian, C.; Chen, L.; *Microchim. Acta* **2019**, *186*, 450.

69. Timbola, A. K.; Souza, C. D.; Soldi, C.; Pizzolatti, M. G.; Spinelli, A.; *J. Appl. Electrochem.* **2007**, *37*, 617.

70. Stefano, J. S.; de Lima, A. P.; Montes, R. H. O.; Richter, E. M.; Muñoz, R. A. A.; *J. Braz. Chem. Soc.* **2012**, *23*, 1834.

71. Lin, K.-C.; Hong, C.-P.; Chen, S.-M.; *Int. J. Electrochem. Sci.* **2012**, *7*, 11426.

72. Kumar, M. A.; Patnaik, S. G.; Lakshminarayanan, V.; Ramamurthy, S. S.; *Anal. Lett.* **2017**, *50*, 350.

73. Prasanna Kumar, S.; Parashuram, L.; Suhas, D. P.; Krishnaiah, P.; *Mater. Sci. Energy Technol.* **2020**, *3*, 159.

74. Pisoschi, A. M.; Pop, A.; Serban, A. I.; Negulescu, G. P.; *J. Electroanal. Chem.* **2012**, *671*, 85.